International Journal of Hydrogen Energy 59 (2024) 874–879

Contents lists available at ScienceDirect

International Journal of Hydrogen Energy

journal homepage: www.elsevier.com/locate/he

Evaluation of the impact of gaseous hydrogen on pipeline steels utilizing hollow specimen technique and μCT

Florian Konert [a,*], Frank Wieder [a], Jonathan Nietzke [a], Dietmar Meinel [a], Thomas Böllinghaus [a], Oded Sobol [a]

[a] Bundesanstalt für Materialforschung und -prüfung (BAM), Unter den Eichen 87, 12205, Berlin, Germany

ARTICLE INFO

Handling Editor: Ramazan Solmaz

Keywords:
Hydrogen embrittlement
Hollow specimen technique
Ferritic steel
In-situ testing
Slow strain rate testing
μCT
Nondestructive testing
Compressed gaseous hydrogen

ABSTRACT

The high potential of hydrogen as a key factor on the pathway towards a climate neutral economy, leads to rising demand in technical applications, where gaseous hydrogen is used. For several metals, hydrogen-metal interactions could cause a degradation of the material properties. This is especially valid for low carbon and high-strength structural steels, as they are commonly used in natural gas pipelines and analyzed in this work.

This work provides an insight to the impact of hydrogen on the mechanical properties of an API 5L *X*65 pipeline steel tested in 60 bar gaseous hydrogen atmosphere. The analyses were performed using the hollow specimen technique with slow strain rate testing (SSRT). The nature of the crack was visualized thereafter utilizing μCT imaging of the sample pressurized with gaseous hydrogen in comparison to one tested in an inert atmosphere.

The combination of the results from non-conventional mechanical testing procedures and nondestructive imaging techniques has shown unambiguously how the exposure to hydrogen under realistic service pressure influences the mechanical properties of the material and the appearance of failure.

1. Introduction

Hydrogen plays a major role in the transition of the European energy supply towards a CO_2 emission-free economy [1]. Structural materials, such as low-alloyed steels, are commonly used for the distribution of hydrogen, e.g. for the majority of natural gas infrastructure components [2]. Along the intention of Europe to blend and transport hydrogen in the existing infrastructure, the relevance of these steels is increasing. In this manner, under specific circumstances, hydrogen can be absorbed into the material and lead to degradation of the mechanical properties manifested mainly through the loss of ductility and facilitation of crack initiation and propagation in the material [3–6], especially in low-alloyed structural steels [7–11]. This process is commonly defined as hydrogen embrittlement (HE) or hydrogen assisted cracking (HAC) and has been the subject of debate for several decades [12].

Elucidation of crack initiation, development and determination of the influence of hydrogen on the mechanical properties are essential to establish lifetime assessments and further understanding of the active mechanisms by combining them with existing theories and models for hydrogen embrittlement.

The operation of classic mechanical tests under gaseous hydrogen atmosphere can be performed in autoclaves to investigate its effect on the mechanical properties. For this method there are guidelines and standards available, as they are given e.g. in ASTM G142 [13] or ISO 11114–4 [14]. Despite the available standard procedures, there are several drawbacks of this technique. The standard procedure includes the use of relatively high volume of hydrogen, which is needed to pressurize an autoclave, this test method holds safety risks which must be managed by time and high costs to cover the risks during an operation of the test in a laboratory. These efforts do not go hand in hand with the essential rapid qualification of materials for the market ramp-up via the need of numerous tests. In the last decade, several researchers worldwide developed a different approach to perform tests in hydrogen atmosphere in a faster, easier and more applicable way, with less safety measures necessary – the hollow specimen technique. Here, by modifying the geometry of the test piece, the specimen itself acts as a containment for the pressurized gaseous atmosphere [15]. This function is gained by the fabrication of a longitudinal hole in the center of the sample (Fig. 1). The main advantage of this technique is the fact that an autoclave is not needed to expose the sample to a pressurized gaseous

* Corresponding author.
E-mail address: florian.konert@bam.de (F. Konert).

https://doi.org/10.1016/j.ijhydene.2024.02.005
Received 20 November 2023; Received in revised form 27 December 2023; Accepted 1 February 2024
Available online 11 February 2024

hydrogen atmosphere. Several investigations have shown, how this technique in various modifications can asses the impact of hydrogen atmospheres on the material properties in comparison to reference atmosphere [16–20].

Based on the mentioned advantages of the hollow specimen technique, this approach is used in this study to investigate the influence of pressurized hydrogen on the material properties and the cracking behavior of a ferritic pipeline steel. Here we present the investigation of the adopted specimen geometry, slow strain rate testing (SSRT) and micro X-ray computed tomography (μCT). The specimens were extracted from a pipeline section.

2. Experimental methods

The samples for the investigations were machined out of a longitudinal welded pipe made of *X*65, which is comparable to L450 in European standard DIN EN ISO 3183 [21]. The concentration of alloying elements was measured by Spectrotest Optical Emission Spectroscopy (SPECTRO GmbH, Kleve, Germany), given in Table 1 and is within the required range. According to the manufacturer, the pipe was assembled by applying submerged-arc welding process on a 28.58 mm sheet, which was delivered in a quenched and tempered condition. The samples were extracted from the base metal far from the weld seam to exclude any influence by the weld metal or the heat affected zone (HAZ).

The samples are orientated longitudinally to the pipe axis. The outer geometry of the samples was machined by turning and the outer surface was machined by grinding afterwards. The inner hole was manufactured by conventional drilling. In order to be able to manufacture the sample internally, a diameter of 3 mm was chosen for the inner hole. The diameter of 3 mm also enables an easy surface measurement. The average roughness of the hole is $R_a = 2.1$ μm and $R_z = 11.7$ μm. Whereas R_a is the calculated mean value of all deviations of the roughness profile from the center line of the defined reference section and R_z describes the mean value of the maximum height differences of 5 consecutive individual measurement sections in the roughness profile. The sample geometry is shown in Fig. 1.

The slow strain rate tensile tests were performed with a 100 kN Cormet machine (Cormet, Vantaa, Finland). Before testing, the samples were rinsed in Acetone with a purity of 99.8 %, the hole was mechanically cleaned and afterwards rinsed in Ethanol with a purity of 99.2 %. Before assembling the samples, they were dried in a nitrogen flow. The samples were filled with hydrogen in a purity of at least 99,999 % hydrogen (Linde GmbH, Pullach, Germany). As a first step before filling each sample, it was evacuated to a pressure of $5*10^{-3}$ mbar. Afterwards the sample was purged 6 times, where in each purging cycle hydrogen was filled to 60 bar and released to 10 bar. After the last purging cycle, the sample was filled up to the test pressure, which was, in accordance with a realistic service pressure of a hydrogen pipeline, also defined as 60 bar. The mechanical loading was started immediately after the sample was filled with hydrogen. The overall duration of the purging and filling process was about 5 min. Tests were performed with a constant displacement rate of 15.24 μm/min, which is equivalent to a nominal strain rate of $1*10^{-5}$ s^{-1}.

After testing, the fracture surface was imaged using a Keyence VHX 5000 (Keyence, Osaka, Japan) digital light microscope to gain overview images and to determine the cross-section-areas after fracture.

The measured values are used to calculate the reduction of area (RA) using Eq. (1):

$$RA\ [\%] = \frac{A_0 - A_f}{A_0} * 100 \quad (1)$$

Where A_0 is the nominal cross section of the specimen and A_f the cross section after fracture. It has to be mentioned that the area of the hole is subtracted and therefore not part of the cross-section. Furthermore, the averaged reduction of areas was used to determine the Embrittlement Index (EI), defined in Eq. (2):

$$EI\ [\%] = \frac{RA_{\ ref} - RA_H}{RA_{ref}} * 100 \quad (2)$$

Where RA_{ref} describes the reduction of area in reference atmosphere and RA_H describes the reduction of area for the samples tested in hydrogen.

Detailed analyses of the fracture surface, fracture type and identification of the different zones were conducted using a Phenom XL scanning electron microscope (SEM, Thermo-Fisher Phenom, Eindhoven, Netherlands) acquired with CeB_6 source. The images were taken using secondary electron detector and acceleration voltage of 15 kV.

Two types of tests were performed using the SSRT. In the first round, tests were performed using hydrogen and argon (as reference) until a complete fracture occurred (resulting in two halves of the specimen). This means that the force decreased from the ultimate yield force to 0 (equivalent to 100 % decrease in force). These tests provided a complete force-displacement behavior of the sample. In the second round of tests, samples (with hydrogen or argon) were strained to a point before fracture. The second round enabled to identify the regions where the

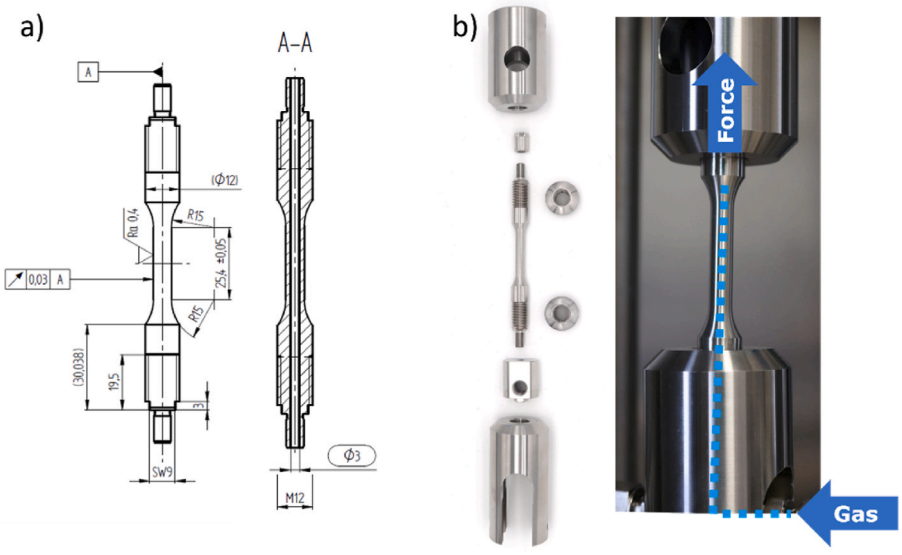

Fig. 1. a) Sketch of the specimen including dimensions and b) sample assembly.

Table 1
Measured chemical composition and nominal composition according to API Specification 5L PSL 2 [22].

	C	Si	Mn	P	S	Cr	Cu	Mo	Ni	Nb	V	Ti	Nb + V + Ti
Measured	0.04	0.31	1.31	0.008	<0.002	0.05	0.02	0.21	0.44	<0.01	0.04	<0.01	<0.05
Nominal	≤0.18	≤0.45	≤1.7	≤0.025	≤0.015	≤0.5	≤0.5	≤0.5	≤0.5	–	–	–	≤0.15

cracks initiate, the nature of crack opening and the path of crack propagation in the bulk using μCT as a nondestructive test method. For the reference sample in argon the test was stopped at a load of 8000 N (28 % decrease in force), whereas the sample, tested in hydrogen, was stopped at a load of 12,000 N (14 % decrease in force). The nominal values of the decreased forces are given in Table 2 and approximated points of the abort are indicated by red dots in Fig. 2.

It must be noted that the different loading levels in the second round were selected based on results from previous tests with hydrogen samples at a decreased load of 8000 N. These tests indicated that the crack has already penetrated the complete wall thickness at a certain spot in the circumference.

Subsequently to the termination of the mechanical loading the gas was released, and the samples were disassembled from the SSRT-machine. After the abortion, the samples were investigated using μCT. The fundamentals of X-ray computed tomography are described in several textbooks [23,24] and are omitted here. Two systems were used for the X-ray tomographic measurements of the hollow tensile specimens. The specimen tested with hydrogen was examined with the commercial 3D X-ray microscope "ZEISS Xradia 620 Versa" (Carl Zeiss AG, Oberkochen, Germany). The X-ray tube in this system is a microfocus X-ray tube from the manufacturer Nordsen DAGE "QuadraNT" with a focal spot of 0.95 μm. To take account of the high density of the hollow tensile specimen, the acceleration voltage was 130 kV, with a power of 19.5 W. The projections were recorded with the flat panel X-ray detector (FPX) "Dexela 2315N2" (CsI scintillator, 3072 × 1944 pixel, pixelpitch: 75 μm). Since the X-ray tube emits a cone beam, appropriate selection of the distance from the tube to the detector, as well as the distance from the tube to the sample, result in a reconstructed voxel size of 5 μm. The data reconstruction was performed using the internal reconstruction software ZEISS Reconstructor. A prefilter was used to reduce beam hardening (caused by the polychromatic X-ray beam). To achieve a sufficient signal-to-noise ratio (SNR), 2400 projections were acquired with 2.26 s exposure time per projection. The data was visualized, processed and analyzed using the commercial software VG Studio Max version 3.4.5 (Volume Graphics, Heidelberg, Germany, 3 2021).

The sample tested in Argon was examined using a system which is an in-house development in cooperation with the company Sauerwein Systemtechnik, today RayScan Technologies GmbH (Meersburg, Germany). The X-ray source is a microfocus X-ray tube XWT-225-SE from X-Ray WorX GmbH (Garbsen, Germany) with a focal spot of 6 μm. The detector is made by PerkinElmer Inc. (Waltham, MA, USA), bears the designation XRD1620 (CsI scintillator, 2048 × 2048 pixel, pixel pitch: 200 μm) and is supplemented with a self-built water cooling system. To ensure the comparability of the results, the measurements were carried out on both devices with the same parameters.

3. Results and discussion

The comparison between the test of a sample filled with gaseous hydrogen and one tested with argon is shown in Fig. 2. The force-displacement curves indicate clear differences between the samples. The two curves are mostly qualitative representative for the tested configurations. The elastic regime in the force-displacement curve is unaffected either by hydrogen or by argon. Moreover, no hydrogen related influence on the yield point of the material has been observed in all tested samples. Furthermore, for the experimental conditions given (room temperature and 60 bar) the ultimate tensile strength (UTS) is not affected by the presence of hydrogen. This is in accordance to the results of Michler et al. for an API 5L *X*60 M steel [18] and other steels consisting of mostly ferritic microstructure [25] tested at room temperature and 100 bar hydrogen. The most significant difference is observed in the maximum elongation. While the reference sample with argon is elongated to 5.2 mm, the sample tested with hydrogen failed at an elongation of 2.9 mm: This indicates a significant loss of ductility, which has been shown for these types of steels under hydrogen atmosphere [7,8,16–18,26,27].

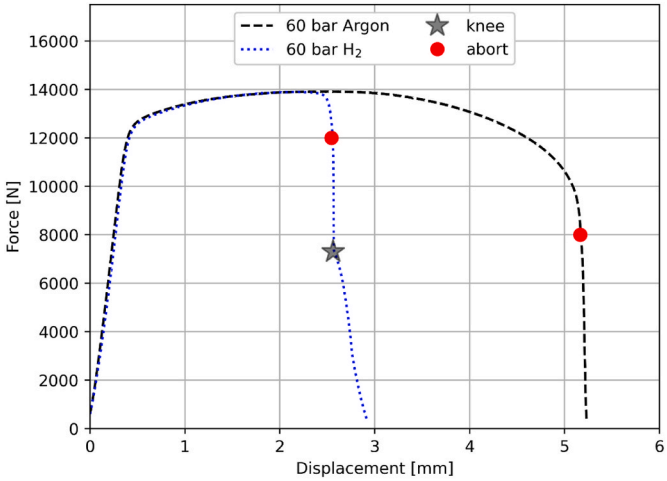

Fig. 2. Force-displacement curve of hollow specimens tested in argon and hydrogen.

Another visible phenomenon has been observed in addition to the quantitative differences in the maximum displacement. In the region which describes the fracture of the specimen, the reference sample shows a smooth and constant decrease of the force gradient. In contrast to the sample tested with argon, the curve describing the fracture process can be divided into two regions for the sample tested with hydrogen. The change from one region to the other is indicated by an asterisk in Fig. 2. The first region (before the asterisk) is characterized by a strong gradient in the decrease of force and therefore in a certain sense have the same nature as the curve of the reference sample. Contrary to the reference sample this gradient is not constant until fracture but is significantly decreased at a medium level of force, indicated by a knee in the Force-Displacement-Curve. It has to be mentioned, that for different samples tested in hydrogen, the value of this force level highly scattered. It is assumed that the knee indicates the point in which the crack reaches the outer surface of the specimen at a certain direction. This behavior can be compared to observations of crack propagation in conventional tensile tests of materials with ductile behavior after a "cup bottom" formation [28]. For the fracture behavior of tubes, Lange [29] has shown the relationship between the appearance of rapid decrease in force and the evolution of fracture surface orthogonal to the highest

Table 2
Nominal forces for the test abortion.

	Round I	Round II
Hydrogen	0 N (fracture)	12,000 N
Argon	0 N (fracture)	8000 N

tensile stress.

Following the tensile tests, samples from the first round of tests (with a complete failure) were analyzed by light microscopy and SEM to characterize the fracture surface and are shown in Fig. 3. The images emphasize the differences between the samples tested with hydrogen and the ones tested with Ar. The reference sample shows a fully ductile fracture across the complete fracture surface area (Fig. 3a). The proof of a ductile fracture, shown in Fig. 3b, affiliated with a typical dimple structure. This type of fracture is common for the tested steel with no hydrogen. This type of fracture has also been shown in conventional tensile tests and tests with hollow specimens by other authors such as Boot et al. Michler et al. and Alvaro et al. [17,18,27]. In contrast to the reference sample, the sample tested in hydrogen shows two different regions divided by their distance to the inner hole. The region closer to the inner hole appears to be reflective in the light microscope image (Fig. 3d), whereas the other region with a bigger distance to the inner hole has a mat appearance. The differences between the two regions are shown in more detail in the SEM images (in Fig. 3c and e). Similarly to the fracture surface of the reference sample, the matt region of the fracture surface in the sample with hydrogen shows dimples as well (Fig. 3c). The region closer to the inner hole is characterized by quasi-cleavage fracture (Fig. 3e). This type of fracture indicates a clear change in the material's properties and the influence of hydrogen, as it was shown by other authors in the last decade [8,17,18,26].

Considering the different types of fractures (i.e. regions) in the sample tested with hydrogen, it is assumed that the change in the fracture nature is due to the expected loss of hydrogen during the test. This assumption is supported by the fact that the crack does not propagate fully concentric over the whole surface but reaches the outer surface of the sample at a confined area. Also Lee et al. [16] reported a transition zone for hollow samples, tested filled with gaseous hydrogen. It is assumed, that as soon as hydrogen is released from the sample through the most developed crack, there is no further uptake of hydrogen into the material. Therefore, hydrogen does not affect the material and the material's behavior returns to a ductile behavior. Therefore, the outer part of the fracture surface shows the formation of dimples at a bigger distance from the inner hole, which indicates a ductile behavior.

All measured and calculated values for the cross-section after fracture, the RA and the EI are summarized in Table 3. Each configuration was tested 3 times. Here, the measured cross-section after fracture indicates a clear loss in ductility due to the presence of hydrogen atmosphere. While the RA in the reference sample tested with argon is 72 %, the samples tested with hydrogen show a RA of 42 %. This result provides an EI of 41 %, which indicates a clear susceptibility of the material to HE.

As mentioned above, the step beyond the state of the art has been achieved by combining the hollow specimen technique with an imaging technique to obtain a more detailed understanding of the crack propagation in the bulk during the tensile test, μCT-investigations were performed to gain a visualization, without damaging the strained specimens, of the development of the cracks, which are leading to the failure of the samples. The results are shown in Fig. 4.

Table 3
Data of SSRT tests expressed in cross-section after fracture, RA and EI.

	Reference	60 bar hydrogen
Cross-section after fracture [mm^2]	6,87 ± 0,36	14,17 ± 0,37
Reduction of Area [%]	72 ± 1,52	42 ± 1,5
Embrittlement Index [%]	–	41

While the reference sample shows a pronounced area where necking occurs (Fig. 4a and c), the sample tested in hydrogen does not show the formation of necking (Fig. 4b and d). As described above, the tests were stopped at different force levels (see Table 2). Despite these differences in both samples, a significant crack is observed. The crack propagation is directly related to high stress concentration at the crack tip. Therefore, it is assumed that no significant further necking can occur during the test until the sample is fully fractured. Li et al. [30] investigated this behavior using a Finite-Element model to describe the necking formation process in metal tubes of various dimensions. The simulations have shown that there is no significant change in the necking after a crack is initiated. Taking this into account, the differences in the necking shape shown in Fig. 4d compared to the necking behavior in the reference sample shown in Fig. 4c, can be associated to the presence of hydrogen. In addition to the different appearance of the necking region, the number of secondary cracks as well as the orientation of the cracks are different between the two samples. The reference specimen has one visible crack which propagates in 45° to the longitudinal axis of the sample, which is the direction of applied mechanical load. The orientation of 45° is the direction of the highest shearing stress [28]. The formation of crack along the plane of the highest shearing stress indicates a ductile behavior of the material [31]. Under this orientation the sample fails by a classic sheared cone fracture, as it is also described by Lange [29]. On the other hand, the sample tested in hydrogen shows one dominant crack which propagates orthogonal to the loading direction and some additional visible secondary cracks. Comparing Fig. 4c and d and , the inner surface of the hydrogen sample seems to have a higher roughness than the reference sample. Considering that both samples were manufactured the same way, it is assumed that the higher inner roughness of the sample tested with hydrogen is due to the presence of hydrogen during the mechanical loading. A possible reason could be the formation of multiple secondary cracks at the inner surface. It is assumed that the starting point of these cracks is given by grooves in the inner surface, produced by manufacturing of the hole [17] by drilling. The growth of a dominant crack is assumed to occur due to inhomogeneities or local stress concentrations in the inner wall resulting

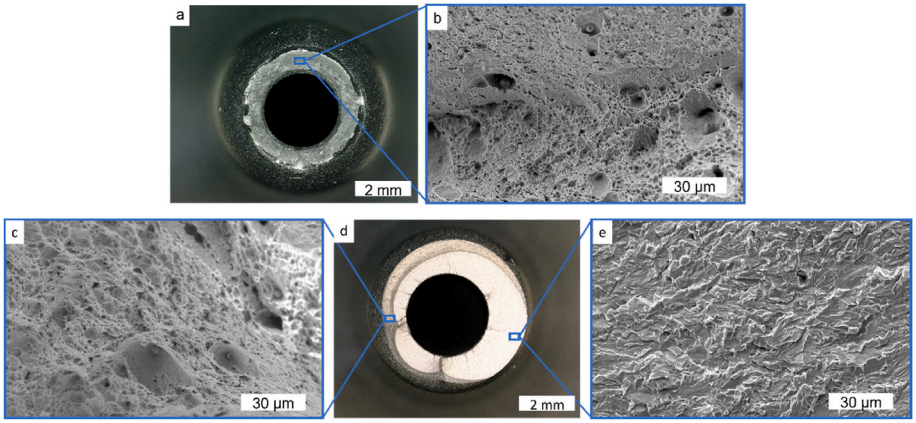

Fig. 3. Fractographic analysis of fractured tensile specimen a), b) specimen tested in 60 bar Argon c), d), e) specimen tested in 60 bar hydrogen.

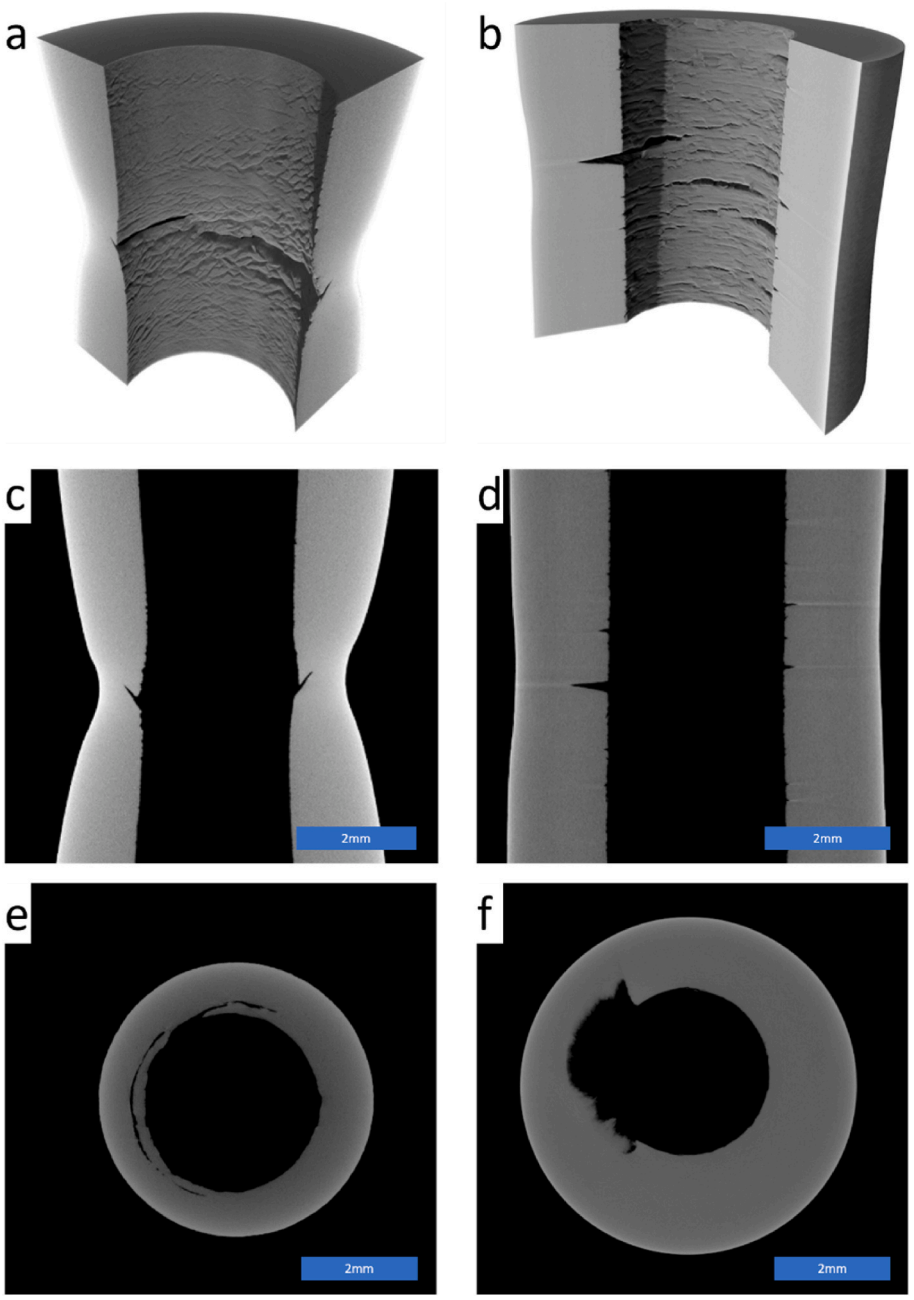

Fig. 4. µCT images of a), c) and e) sample loaded in Argon and b), d) and f) sample loaded in hydrogen.

in a favorable notch, which becomes later the dominant crack and develops further. Another difference is the crack propagation path. While the crack in the sample tested with argon (reference) seems to propagate in a nearly symmetric way, the crack in the sample tested with hydrogen propagates in a preferred direction. On one hand this is shown by the different length of the crack over the circumference of the hollow specimen as it is shown in Fig. 4 comparing Fig. 4c and d. This is also shown by the comparison of Fig. 4e and f and. While the cross-section of the sample tested in Argon (Fig. 4e) is nearly symmetrical, the cross-section of the sample tested in hydrogen (Fig. 4f) is characterized by a localized material separation indicated by the black regions.

4. Conclusions

The hollow specimen technique presented in this work is shown as a useful tool which can facilitate experiments to observe the effects of pressurized gaseous hydrogen on the mechanical properties of metallic materials. The results showed how using much smaller volume of hydrogen within the sample is sufficient to result in a reduction of ductility of the tested *X*65 pipeline steel. The effectiveness of this method is also emphasized by fractographic analyses in which the susceptibility of the material to hydrogen embrittlement has been observed by the formation of quasi-cleavage fracture for the sample tested with hydrogen.

This work presents a novel combination of tools to visualize the crack propagation in ferritic steel under gaseous hydrogen atmospheres. The easily applicable and therefore promising method of the hollow specimen technique was utilized and combined with the nondestructive X-Ray. This provided a unique insight into the process of crack formation and growth and should be further developed by analyzing more steps in the failure process. The images showed significant change in the crack orientation in samples tested with hydrogen compared to samples tested

in reference atmosphere. In addition, the number of secondary cracks is much higher in the samples tested in a hydrogen atmosphere. After nucleation of several cracks, one crack masters the crack propagation leading to the final fracture and failure of the sample. This crack is oriented orthogonal to the tensile loading direction and its progress is asymmetrical across the bulk surrounding the inner hole.

As a first step, the analyses using μCT were performed at an intermediate stage of the tensile test. With the existing tools it is possible to perform a following experiment in which the visualization takes place during crack formation. Using such procedure can provide a deeper insight to the mechanisms leading to crack initiation and propagation under hydrogen atmosphere. This step will contribute to a better understanding of the degradation processes in structural materials.

Declaration of competing interest

The authors declare that they have no known competing financial interests or personal relationships that could have appeared to influence the work reported in this paper.

Acknowledgements

The authors would like to thank Eisenbau Krämer GmbH, especially Dr. Iris Rommerskirchen for providing the tested material.

References

[1] Hydrogen roadmap Europe: a sustainable pathway for the European energy transition. Gemeinsames Unternehmen Brennstoffzellen und Wasserstoff; 2019.
[2] Jia G, et al. Hydrogen embrittlement in hydrogen-blended natural gas transportation systems: a review. Int J Hydrogen Energy 2023.
[3] Zhang L, et al. Effect of nickel equivalent on hydrogen gas embrittlement of austenitic stainless steels based on type 316 at low temperatures. Acta Mater 2008; 56(14):3414–21.
[4] Fan YH, et al. Effect of grain refinement on the hydrogen embrittlement of 304 austenitic stainless steel. J Mater Sci Technol 2019;35(10):2213–9.
[5] Rozenak P, Eliezer D. Effects of metallurgical variables on hydrogen embrittlement in AISI type 316, 321 and 347 stainless steels. Mater Sci Eng 1983;61(1):31–41.
[6] Ye F, et al. Effects of dislocations and hydrogen concentration on hydrogen embrittlement of austenitic 316 stainless steels. J Alloys Compd 2021;876:160134.
[7] Wang D, et al. Investigation of hydrogen embrittlement behavior in X65 pipeline steel under different hydrogen charging conditions. Mater Sci Eng 2022;860: 144262.
[8] Ranjbar M, et al. Effect of microstructure on the mechanical properties and fracture toughness of API X65 pipeline steel in the presence of hydrogen. Met Mater Int 2021;27(10):3918–34.
[9] Mendibide C, et al. Effect of degraded environmental conditions on the service behavior of a X65 pipeline steel not designed for hydrogen transport. Int J Hydrogen Energy 2023.
[10] Laureys A, et al. Use of existing steel pipeline infrastructure for gaseous hydrogen storage and transport: a review of factors affecting hydrogen induced degradation. J Nat Gas Sci Eng 2022;101:104534.
[11] Depraetere R, et al. Influence of stress triaxiality on hydrogen assisted ductile damage in an X70 pipeline steel. Mater Sci Eng 2023;864:144549.
[12] Robertson IM, et al. Hydrogen embrittlement understood. Metall Mater Trans B 2015;46(3):1085–103.
[13] ASTM G142. *Standard test Method for Determination of Susceptibility of Metals to Embrittlement in hydrogen containing Environments at high pressure, high temperature, or both* ASTM international. ASTM International; 1998.
[14] DIN EN ISO 11114-4, Ortsbewegliche Gasflaschen – verträglichkeit von Werkstoffen für Gasflaschen und Ventile mit den in Berührung kommenden Gasen – teil 4: prüfverfahren zur Auswahl von Stählen, die gegen Wasserstoffversprödung unempfindlich sind *(ISO 11114-4:2017); Deutsche Fassung EN ISO 11114-4:2017* DIN Deutsches Institut für Normung e.vol. 2017, Beuth Verlag GmbH: Berlin.
[15] Chandler W, Walter R. Testing to determine the effect of high-pressure hydrogen environments on the mechanical properties of metals. ASTM International; 1974.
[16] Lee Y-H, et al. Mechanical degradation of API X65 pipeline steel by exposure to hydrogen gas. Met Mater Int 2011;17(3):389–95.
[17] Boot T, et al. In-situ hollow sample setup design for mechanical characterisation of gaseous hydrogen embrittlement of pipeline steels and welds. Metals 2021;11(8): 1242.
[18] Michler T, et al. Comparison of tensile test results in high pressure gaseous hydrogen using conventional and tubular specimens. In: Pressure vessels and piping conference. American Society of Mechanical Engineers; 2021.
[19] Ogata T. Simple mechanical testing method to evaluate influence of high pressure hydrogen gas. In: Pressure vessels and piping conference. American Society of Mechanical Engineers; 2018.
[20] Ogata T. Influence of high pressure hydrogen environment on tensile and fatigue properties of stainless steels at low temperatures. 2012. p. 39–46.
[21] DIN EN ISO 3183. *Erdöl- und Erdgasindustrie – Stahlrohre für Rohrleitungstransportsysteme (ISO 3183:2019); Deutsche Fassung EN ISO 3183:2019* DIN Deutsches Institut für Normung e.V. Berlin: Beuth Verlag GmbH; 2020.
[22] Line pipe API SPECIFICATION 5L, American petroleum institute. Washington: American Petroleum Institute; 2018.
[23] Slaney M, Kak A. Principles of computerized tomographic imaging. IEEE press; 1988.
[24] Buzug TM. Computed tomography. In: Springer handbook of medical technology. Springer; 2011. p. 311–42.
[25] Michler T, Ebling F. Einfluss von Hochdruckwasserstoff auf die Zugversuchseigenschaften von ausgewählten Druckbehälter-und Pipelinestählen. 2021.
[26] Khatib Zadeh Davani R, Miresmaeili R, Soltanmohammadi M. Effect of thermomechanical parameters on mechanical properties of base metal and heat affected zone of X65 pipeline steel weld in the presence of hydrogen. Mater Sci Eng 2018;718:135–46.
[27] Alvaro A, et al. Materials testing and characterization of four X60-X65 pipeline steels. SINTEF Rapport; 2021.
[28] Lange G. Der Ablauf des Bruches in duktilen, zugbeanspruchten Legierungen. Int J Mater Res 1976;67(5):372–9.
[29] Lange G. Bruchformen und Spannungszustände dickwandiger Rohre. Int J Mater Res 1977;68(4):289–92.
[30] Li C, et al. Investigation of the geometry of metal tube walls after necking in uniaxial tension. Metals 2017;7(3):100.
[31] Rösler J, Harders H, Bäker M. Mechanisches verhalten der Werkstoffe. Springer-Verlag; 2012.